Progress In Electromagnetics Research C, Vol. 109, 77–94, 2021

A Low-Profile Dual-Band Base Station Antenna with Antenna on Antenna Structure

Wei Luo[1], Zhixiong Ni[1, *], Yuqi Yang[2], Bo Yin[1], Yi Ren[1], and Wen Huang[1]

Abstract—A low-profile dual-band composite structure antenna is proposed for fifth generation mobile communication system (5G), which is named as Antenna on Antenna (AOA). Loaded with an artificial magnetic conductor (AMC) reflector, the proposed AOA element consists of a pair of dual-polarized lower band (LB) dipole antennas working in the 0.7–1.03 GHz band and four upper band (UB) patch antenna arrays working in the 24.25–27 GHz band, which covers LTE and 5G millimeter wave band. In order to reduce the size of base station antenna, the millimeter wave patch antenna arrays are parasitic on LB dipoles. While the radiator of the LB antenna is utilized as the ground of the millimeter wave patch antenna array, LB and UB antennas share the same dielectric substrate. The profile height of the antenna is reduced by AMC reflector effectively. Meanwhile, the three-element AOA array loaded with AMC reflector is designed to validate the overall performance of base station antenna. The operation bands of the proposed AOA are 0.7–1.03 GHz ($S_{nn} < -14$ dB) and 24.25–27 GHz ($S_{nn} < -10$ dB) for LTE and 5G millimeter bands, respectively. Antenna prototype was fabricated and measured to verify the design solution. The measured results which are consistent with simulated results show that the AOA has good impedance matching, port isolation, and stable radiation pattern.

1. INTRODUCTION

With the development of various generations of wireless mobile communication systems, the coexistence of multi-standard communication systems has become the current focus in the Long Term Evolution (LTE) and 5G communication system [1]. Various standards in the sub-6 GHz bands are reported, such as LTE700 (698–803 MHz), GSM850 (814–894 MHz), GSM900 (890–960 MHz), LTE2300 (2300–2400 MHz), and LTE2500 (2500–2690 MHz). Due to spectral congestion in the sub-6 GHz bands, the communication frequency band has gradually shifted to the millimeter wave band (3GPP FR2: 24.25–52.6 GHz) and is no longer limited to sub-6 GHz [2]. In order to increase the transmission speed of mobile communication to a greater extent, designs of base station at 24 GHz and beyond for 5G cellular systems are presented by researchers in academia. However, the path loss of the millimeter wave communication link is an inevitable obstacle. To ensure the reliability of the communication link, the millimeter wave array antenna is used to compensate the path loss with its high gain beam [3, 4]. In addition to the dual polarizations, high gain, broadband, and low cross-polarization rate required by traditional base station antennas, it is also important to achieve dual-band functions. As a transitional period, the coexistence of 4G and 5G networks will continue for a long time. Consequently, finding a novel integration method for antennas applied to both 4G and 5G networks has remained an elusive challenge [5, 6].

Several dual-band antennas with low frequency ratios and all in sub-6 GHz have been proposed, which are regarded as a feasible approach to resolve this problem [7]. Sharing antenna elements and feed ports in lower-band (LB) and upper-band (UB) is considered as an excellent solution. As presented

Received 1 November 2020, Accepted 11 January 2021, Scheduled 26 January 2021
* Corresponding author: Zhixiong Ni (529423118@qq.com).
[1] College of Electronic Engineering, Chongqing University of Posts and Telecommunications, Chongqing, China. [2] Electronic Information and Networking Research Institute, Chongqing University of Posts and Telecommunications, Chongqing, China.

in [8], the characteristic of double broadband is realized by loading parasitic rings and metal walls on and around the crossed magneto-electric (ME) dipoles. A novel dual-wideband dipole directional antenna with double reflecting floors was proposed in [9], around which four Γ-shaped branches are parasitic around the antenna. In [10], a dual-band loop-dipole composite antenna was proposed, and three operation modes of the antenna were excited at 1.8 GHz, 2.4 GHz, and 5.3 GHz respectively to cover two bands. However, these antennas have the problem of unstable radiation performance.

Another solution is to use separate and independently fed antenna units to achieve dual-band characteristics. Several antenna arrays arranged side-by-side or embedded and sharing one reflector were proposed in [11, 12]. However, when the two operating bands are close or comparable to each other, the low isolation caused by mutual coupling is inevitable. The integration of sub-6 GHz and millimeter wave band antennas can effectively avoid this problem. [13] presented the composite structure of a four-unit linear 28 GHz array and 3.5 GHz dipole antenna by sharing aperture technology. A dual-frequency antenna with a large frequency ratio in the form of independent feed was reported in [14], which was integrated with a microwave parallel-plate waveguide resonator antenna and a millimeter-wave Fabry-Perot resonator antenna.

Miniaturization has become the dominant trend of antennas in wireless communication systems. In addition to the use of dual-frequency/multi-frequency technology, reducing the profile height of the antenna is also of great significance to alleviating the tightness of base station [15]. A method of folding the short-circuit patch in the vertical direction was proposed in [16], which reduces the profile height of the electromagnetic dipole from $0.25\lambda_0$ (λ_0 is the free-space wavelength at central frequency) to $0.116\lambda_0$. In [17], a four-leaf-clover-shaped dielectric resonator antenna, excited by two sets of phase external modes, used its high-permittivity dielectric material to make the antenna profile height only $0.06\lambda_0$. However, the cost of dielectric materials with high dielectric constant cannot be ignored. As mentioned in [18], a differentially fed slot antenna was presented, of which profile height is only $0.13\lambda_0$.

In this paper, a low-profile dual-polarization dual-band composite structure antenna named as antenna on antenna (AOA) loaded with an AMC structure is proposed and analyzed. The LB unit and UB array share a dielectric substrate, and the low frequency unit serves as the ground of the high frequency array to achieve the purpose of dual bands which includes 0.85 GHz for LB and 25.5 GHz for UB. The antenna loaded with the AMC reflector uses the AMC reflector's in-phase reflection characteristics to reduce the overall profile height of the antenna. Moreover, based on the proposed antenna, a three-element antenna array is designed and fabricated to validate the design.

2. ANTENNA ON ANTENNA DESIGN

2.1. Lower Band Dipoles

The configuration of the wideband dual-polarized LB element is shown in Figure 1(a). The antenna consists of two pairs of intersecting leaf-shaped printed planar dipoles, two crescent-shaped coupled feeders, and a metal reflector. As shown in Figure 1(b), each arm of leaf-shaped dipole has two fillets around the corner which have an important influence on the radiation pattern of the wideband dipole. The leaf-shaped dipoles are printed on the bottom side of the substrate which is made of Rogers RO4350 (the relative permittivity is $\varepsilon_r = 3.66$; loss tangent is 0.004; the thickness is 0.508 mm), whereas the crescent-shaped coupling feed lines are printed on the top side of the substrate. The dipoles are fed through a coaxial cable. The inner conductor of coaxial cable is connected to crescent-shaped coupling feed line, while the outer conductor of coaxial cable is soldered on a radiating arm of the dipole.

The two pairs of leaf-shaped dipole antennas are in the form of dual-port feed. The energy is fed into the crescent-shaped coupling feeder through a coaxial cable and then coupled to the dipole radiator to radiate electromagnetic waves. The two pairs of dipoles are placed crosswise along $\pm 45^\circ$ to achieve the function of polarization diversity. When a pair of dipoles are fed, the other pair of dipoles act as resonators. The arm of dipole, which acts as a resonator, is coupled to the main radiator to generate the inverse current at the edge. The reverse current forms a closed loop on the resonator to produce a circular current through the electromagnetic coupling, which induces a new resonator mode. From the current distribution in Figure 2, it can be found that the distribution current intensity of the coupling edge is particularly obvious. The resonant mode is influenced by the fillet R_p due to variation of the current path length. When R_p increases, the high-frequency resonance point and low-frequency

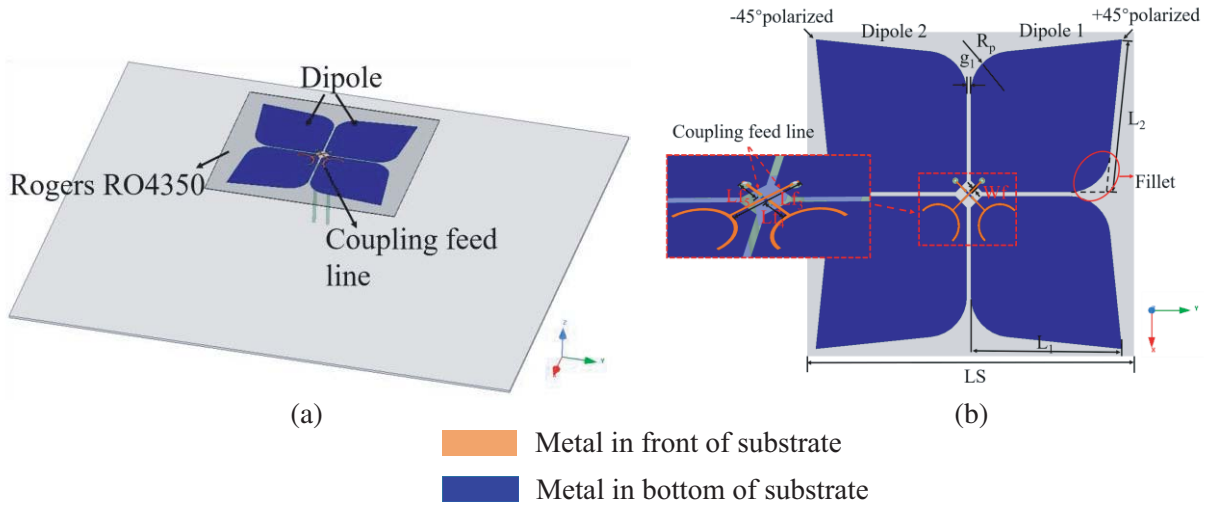

Figure 1. Geometry of the LB dipoles. (a) Overall view; (b) Top view of dipoles and feeding structures. ($LS = 170\,\text{mm}$, $R_p = 15\,\text{mm}$, $g_1 = 2\,\text{mm}$, $L_1 = 68\,\text{mm}$, $L_2 = 68.3\,\text{mm}$, $Lf_2 = 18\,\text{mm}$, $Lf_4 = 8.3\,\text{mm}$, $Lf_5 = 6.7\,\text{mm}$, $Wf = 1.1\,\text{mm}$).

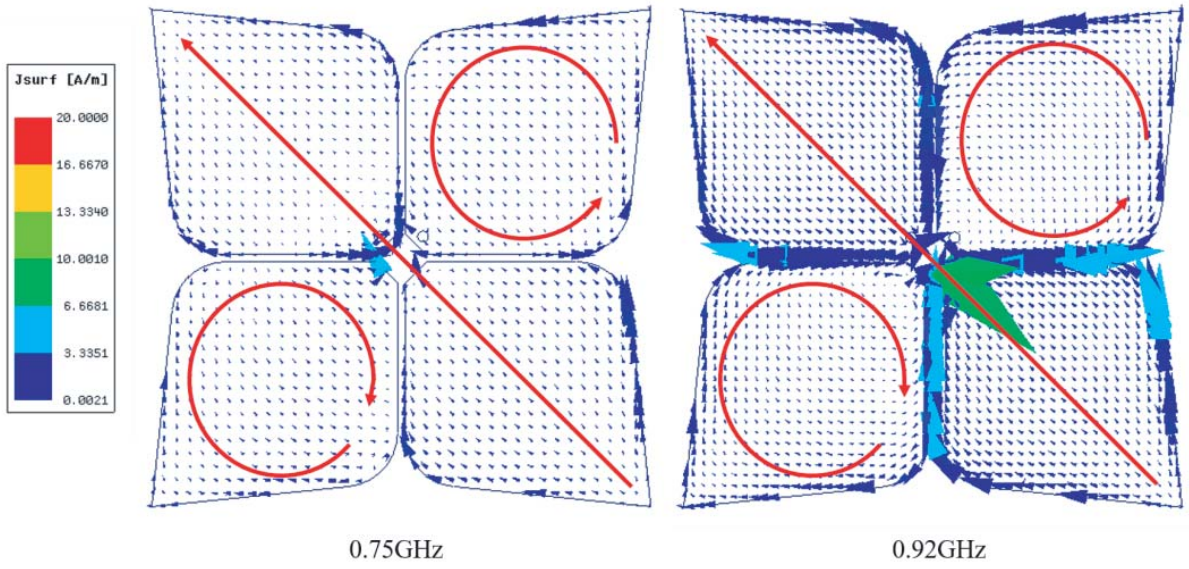

Figure 2. Simulated current distribution of dipoles at 0.75 GHz and 0.92 GHz.

resonance point move in opposite directions toward the two ends, as shown in Figure 3. Thus, the operation band of LB dipole is widened. Due to the extension of current path of the main radiating dipole, the low resonant mode degrades with the increase of R_p. Similarly, the high resonant mode increases with the increase of R_p, since the current path of the radiation edge of the dipole is reduced. Therefore, the miniaturization and broadband of the antenna can be achieved.

2.2. Upper Band Rectangular Microstrip Array

The UB millimeter-wave array antenna is composed of 16 elements (4×4) with an overall size of $35\,\text{mm} \times 35\,\text{mm}$, which is shown in Figure 4(a). Adopting equal power division and parallel connection, the array is fed with a coaxial line. The array is printed on a dielectric substrate made of Rogers RO4350 (the relative permittivity is $\varepsilon_r = 3.66$, and the thickness is 0.508 mm), and the copper is

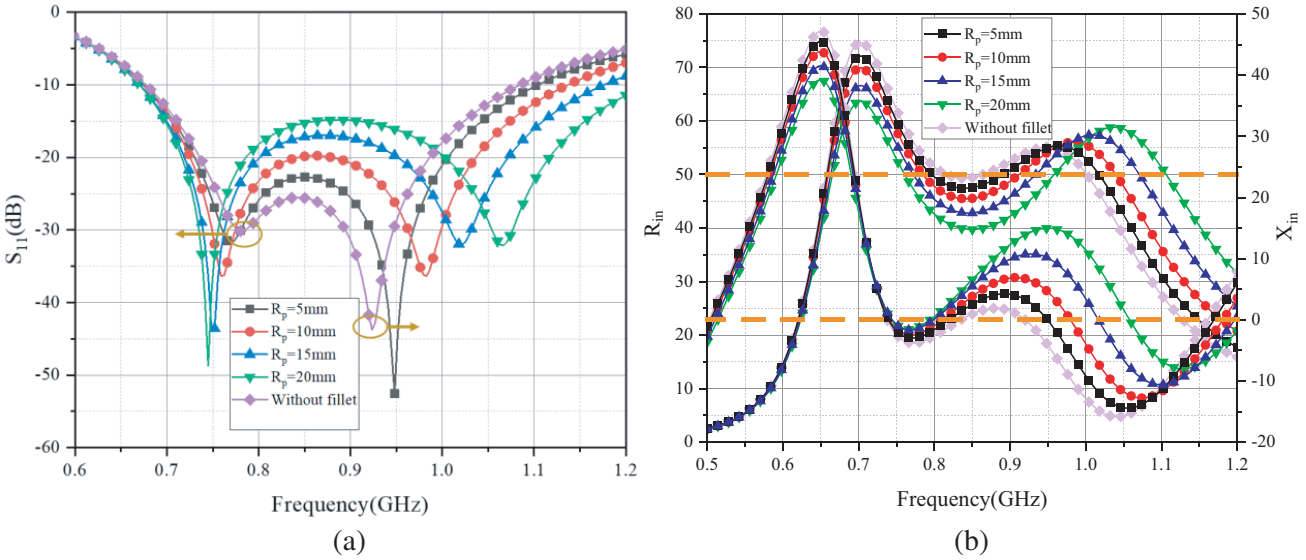

Figure 3. Effects of R_P on the impedance matching. (a) S_{11}. (b) Input impedance.

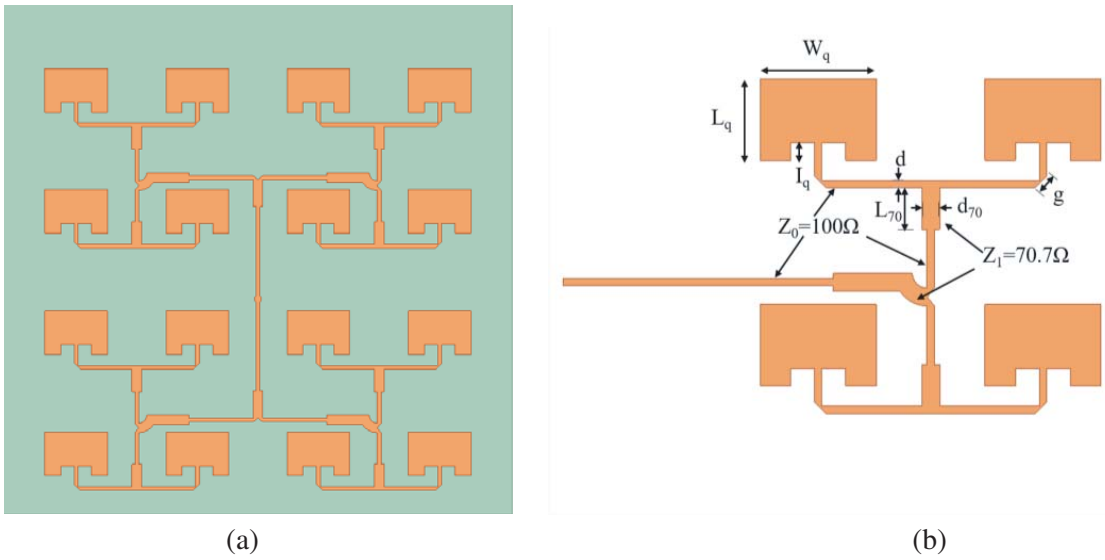

Figure 4. Configuration of 4×4 microstrip patch array antenna. (a) Top view. (b) Detailed size of antenna array. ($W_q = 3.92\,\text{mm}$, $L_q = 2.74\,\text{mm}$, $I_q = 0.61\,\text{mm}$, $L_{70} = 1.41\,\text{mm}$, $d_{70} = 0.6\,\text{mm}$, $d = 0.24\,\text{mm}$, $g = 0.54\,\text{mm}$).

deposited under the dielectric substrate as the ground of the array. Since the user equipment (UE) is near the base station in the 5G millimeter wave band, single-polarization millimeter-wave band base station is suitable for this communication scenarios [19]. The microstrip rectangular patch is utilized as the array unit. Considering the parasitic radiation caused by microstrip line and layout design of the feeder network, the width of $100\,\Omega$ feeder is optimized to 0.24 mm. 2×2 antenna units and feeder networks are shown in Figure 4(b).

In order to prevent the deleterious coupling between the feeder and the upper corner of the patch, it is necessary to introduce a circular arc-shape microstrip line. The 3/4 impedance transformer is utilized to eliminate impedance discontinuities in the circular arc segment. The current flows from the feeding center of the antenna array to each element substantially uniformly, as shown in Figure 5.

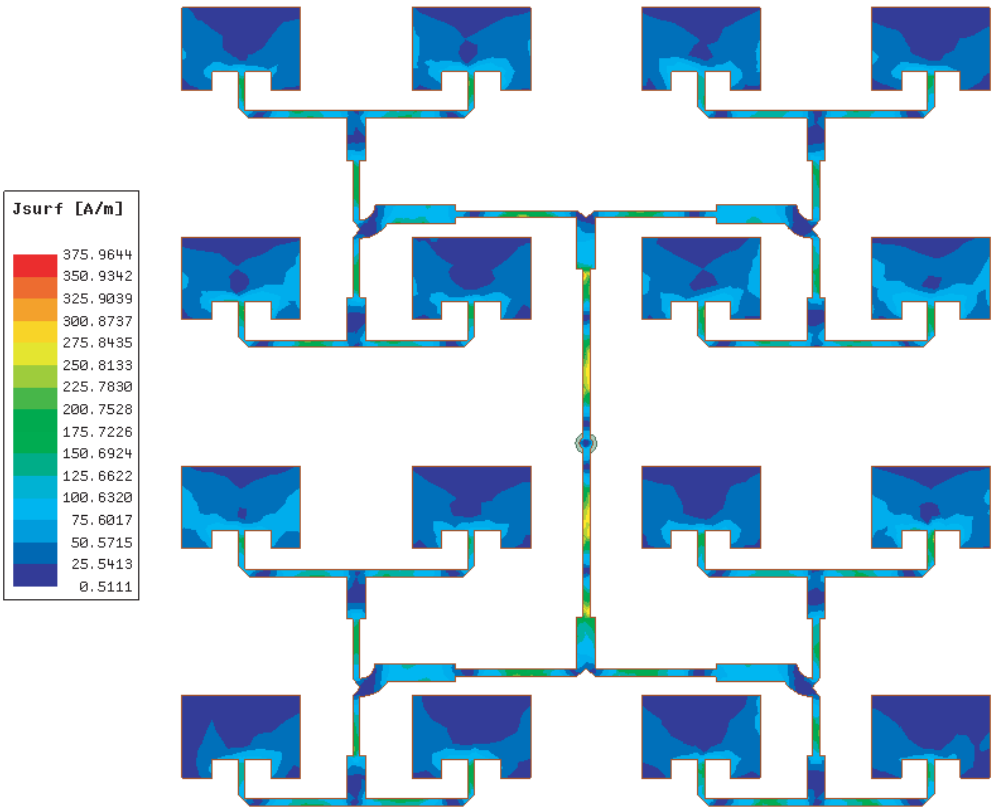

Figure 5. Current distribution of UB array at 26 GHz.

2.3. Composite Structure of Antenna on Antenna

The integrated high and low frequency radiator, named as AOA, is proposed with a high frequency ratio. The UB and LB radiators of AOA share the same substrate which is different from usual dual-frequency antennas in other papers. As shown in Figure 6(a), four pentagrams which represent the UB rectangular microstrip arrays are placed above the four ellipses which represent radiating arms of the LB dipoles. The antenna model of AOA is shown in Figure 6(b).

The layout of antennas in Figure 6 ensures that the radiation performances of the LB dipoles are not affected by the UB arrays. Each arm of LB leaf-shaped dipoles not only radiates electromagnetic waves, but also works as the ground for UB patch arrays. The UB patch arrays and LB dipole antenna are fed independently by four UB ports and two LB ports through coaxial cables, respectively. For LB dipoles, the outer conductor of coaxial cable is soldered on the radiator of dipoles, while the inner conductor is connected to the crescent-shaped coupling feed line. Similarly, the outer conductor of the coaxial cable used to feed the UB array is soldered on the center of the LB dipole radiator.

3. DESIGN OF LOW-PROFILE ANTENNA

3.1. AMC Reflector

The AMC reflector is composed of 6×6 periodically arranged structural units, an FR4 substrate, an air substrate, and an aluminum plate, from top to bottom. Each periodic structural unit consists of a square patch and four 5-shaped grooves which are rotationally etched on the patch. The patch unit etched with a "5"-shaped gap provides inductance L_p, and the gap between patches provides capacitance C_a. The inductance L_s is generated by the structural units and aluminum plate. Figure 7 shows the AMC structure and equivalent circuit model.

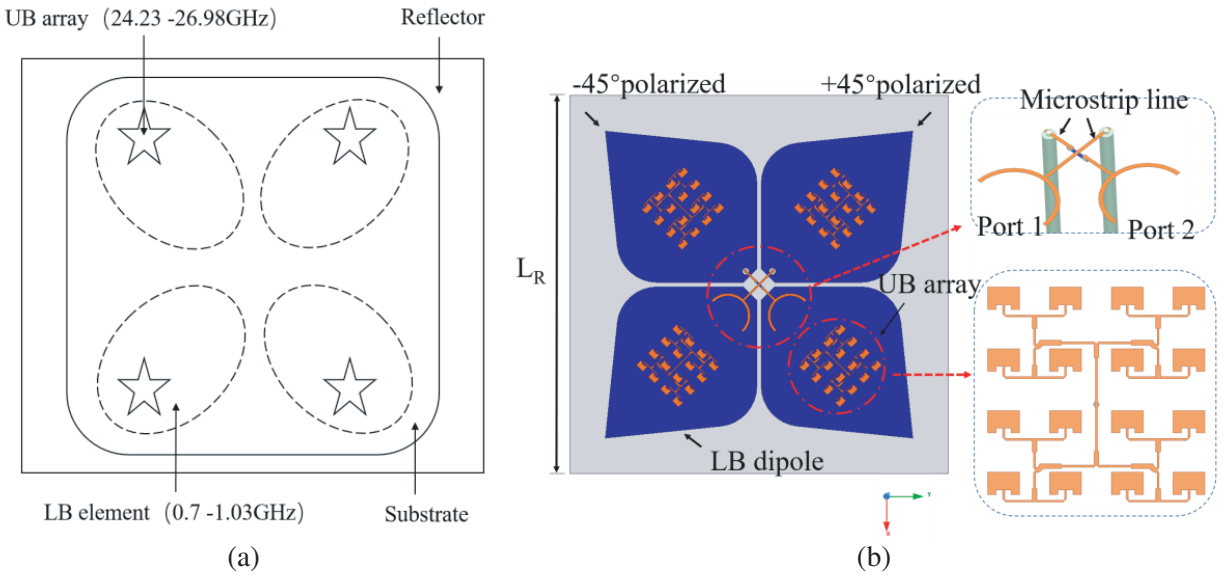

Figure 6. Structure diagram of AOA. (a) Principle scheme. (b) Detailed size of AOA. ($L_R = 170\,\text{mm}$).

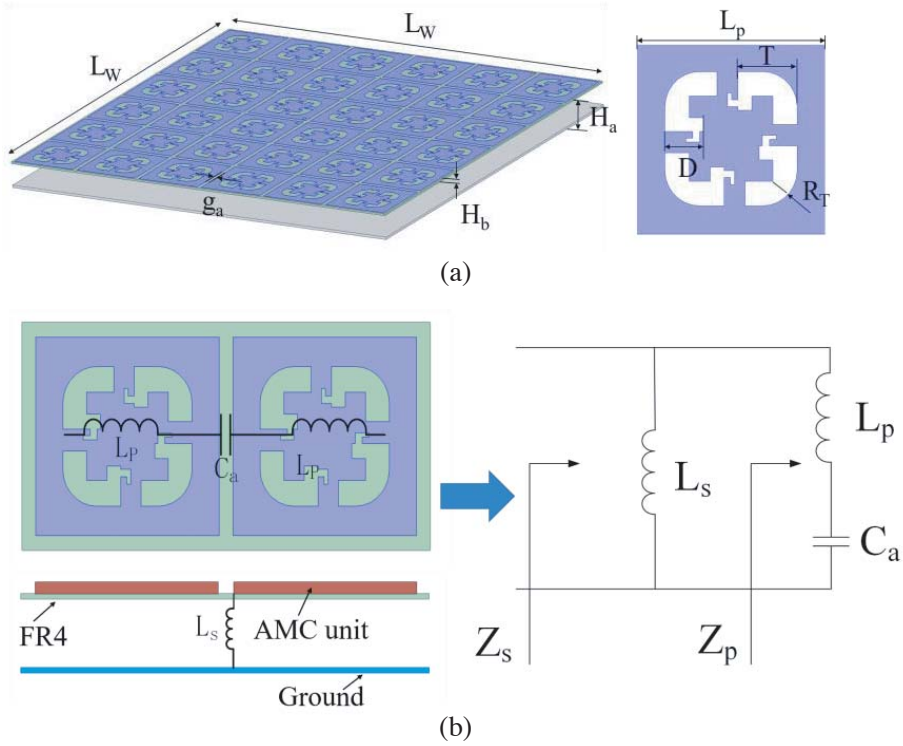

Figure 7. Configuration of AMC reflector. (a) Structure of AMC. (b) Equivalent circuit model of AMC. ($L_W = 448\,\text{mm}$, $g_a = 4\,\text{mm}$, $H_a = 20\,\text{mm}$, $H_b = 1.5\,\text{mm}$, $L_p = 54\,\text{mm}$, $T = 17\,\text{mm}$, $D = 11\,\text{mm}$, $R_T = 10\,\text{mm}$).

The total surface impedance of the AMC reflector is expressed as follows [20]:

$$\eta = Z_{\text{p}} \parallel Z_s = j\omega L_s \frac{1 - \omega^2 L_s C_a}{1 - \omega^2 (L_s + L_p) C_a} \tag{1}$$

where Z_p is the impedance of the periodic structure array, and Z_s is the impedance of the total dielectric

layer. Since the AMC forms a high impedance surface (HIS) at the resonance frequency, the total surface impedance $\eta \to +\infty$. The resonance frequency f_a can be obtained by the following expression:

$$f_a = \frac{1}{2\pi\sqrt{(L_s + L_p)C_a}} \tag{2}$$

There are many ways to study the characteristics of frequency selective surfaces. The reflection coefficient is a key index to evaluate the performance of AMC surface, which is analysed based on the assumption of plane wave incidence.

The thickness H_a of the air layer directly affects the slope of the reflection phase curve. Since the resonance frequency f_a is negatively related to L_s, the relationship between L_s and the thickness of the total dielectric layer is expressed as follows:

$$L_s = \mu_0 \cdot h \tag{3}$$

where μ_0 is the permeability in vacuum.

The expression of the impedance bandwidth (BW) of AMC is as follows:

$$BW = \frac{\pi}{8\eta_0}\sqrt{\frac{L_s + L_p}{C_a}} \times \left(\frac{L_s}{L_s + L_p}\right)^2 \tag{4}$$

It can be clearly seen from Equations (2) and (3) that as the thickness of the air layer H_a increases, the resonant frequency f_a of the AMC will gradually decrease, with the thickness of the dielectric substrate unchanged. Equation (4) shows that BW will increase with the increase of L_s (when $L_s \geq 0$), that is, the in-phase reflection band gap curve tends to be flat from $-90°$ to $90°$. All the above can be verified from the simulation results of reflection amplitude and phase in Figure 8.

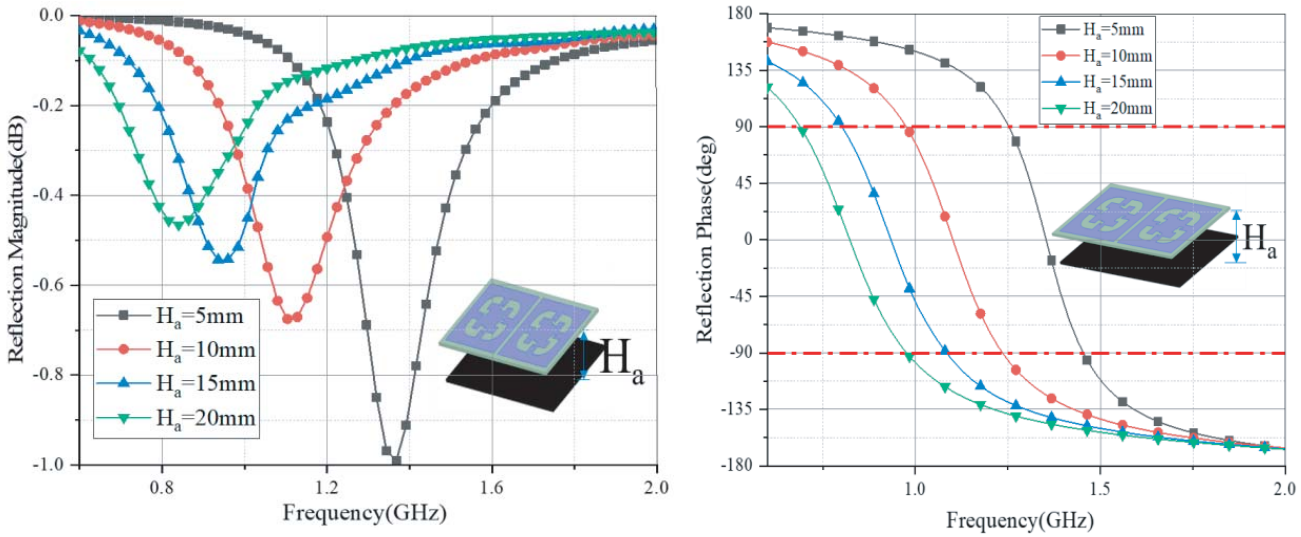

Figure 8. Reflection coefficient of AMC reflector varies with H_a. (a) Amplitude. (b) Phase.

3.2. Low-Profile LB Dipoles Design

As shown in Figure 9, the LB leaf printed planar dipole antenna is placed above the perfect electric conductor (PEC) reflector and AMC reflector, respectively. According to the boundary condition of the ideal conductor, the tangential component of the electric field radiated downward by the dipole is 0 on the surface of the reflector, and the radial incident wave and reflected wave have π phase difference. The electric field above the dipole antenna can be equivalent to the superposition of the radiation wave of the dipole antenna and the reflection wave of the reflector. In order to avoid the inverse superposition

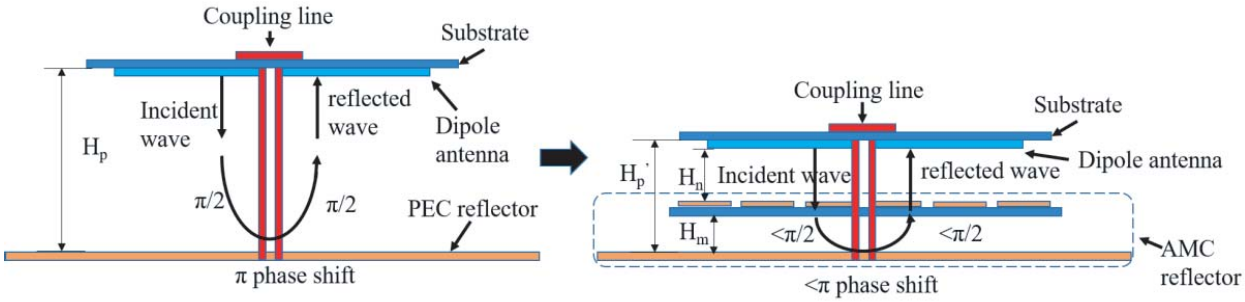

Figure 9. Principle of low profile LB dipole with AMC reflector.

of the two electric fields, H_p is usually close to $\lambda/4$ of the radiation center frequency. However, when the antenna is placed on the AMC reflector, the phase difference between the incident wave and reflected wave is less than π. Since the AMC reflector is equivalent to the ideal magnetic conductor at resonance frequency, the phase difference of the incident wave and reflected wave is 0. Thus, the radiation wave and reflected wave are superimposed in the same phase to enhance the radiation. As a reflector, AMC can realize the reflection phase within $\pm 90°$ in a certain frequency band, that is, in-phase reflection phase band gap. At the center frequency of the frequency band, AMC is equivalent to an ideal magnetic conductor, and the profile height of the antenna will be greatly reduced. Therefore, loading with AMC reflector can realize the low profile characteristics of the antenna.

Based on the LB cross dipole antenna proposed by Section 2, the metal reflector on the back of the antenna is replaced by AMC reflector. Then the distance between the LB dipole antenna and AMC reflector is adjusted to H_n. Good impedance matching is achieved in the original working band, while the profile height is reduced to H_p'. It is found that the profile height is lower than the original antenna in Figure 9.

As shown in Figure 10, for the loaded PEC reflector, the original LB dipole antenna height is reduced from $H_1 = 90\,\text{mm}$ (0.25λ) to $H_1 = 45\,\text{mm}$ (0.125λ), and the impedance matching of the dipole deteriorates sharply. However, for the AMC reflector loaded with the same height $H_1 = 45\,\text{mm}$ (0.125λ), the impedance matching has been significantly improved. The obvious resonance frequency point could be found from the S_{11} curve of AMC reflector. The "green circle" indicates that the impedance matching

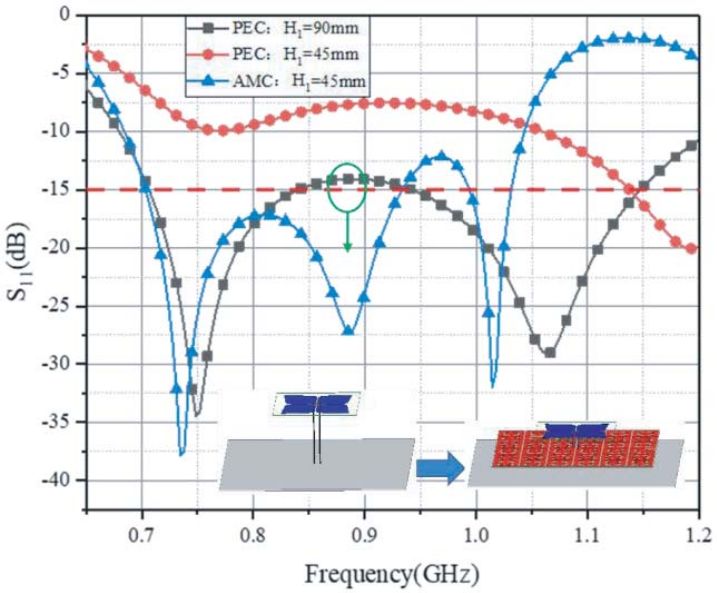

Figure 10. Simulated S_{11} of the LB dipoles antenna backed by PEC and AMC reflectors.

of the LB dipole antenna is improved with the AMC reflector. It could be found that a new resonance mode is generated at 0.88 GHz, which is caused by the interaction of the dipole antenna and the AMC reflector. Therefore, the profile height of the LB dipole antenna using the AMC reflector can be reduced by about 45 mm (50%).

4. SIMULATIONS AND MEASUREMENTS

4.1. Low-Profile AOA Element

The configuration of the proposed AOA loaded with AMC reflector is shown in Figure 11(a). It includes four pairwise orthogonal rectangular microstrip arrays for UB, two pairs of planar printed leaf-shaped crossed-dipoles for LB, and an AMC reflector used to reduce the profile. The UB arrays and LB dipoles are printed on upper and lower sides of the substrate 1 made of Rogers RO4350 (the relative permittivity is $\varepsilon_r = 3.66$, and the thickness is 0.508 mm), as shown in Figure 11(b). Figure 11(c) shows the AMC reflector, which consists of a periodic rectangular slotted patch array, substrate 2, an air layer, and an aluminum plate from top to bottom. Substrate 2 is FR4 with a relative permittivity of $\varepsilon_r = 4.4$, and the thickness is 1.5 mm. The AOA and AMC surface are placed at heights of $H_1 = 45$ mm ($0.125\lambda_0$) and $H_3 = 20$ mm ($0.05\lambda_0$), from the aluminum plate respectively.

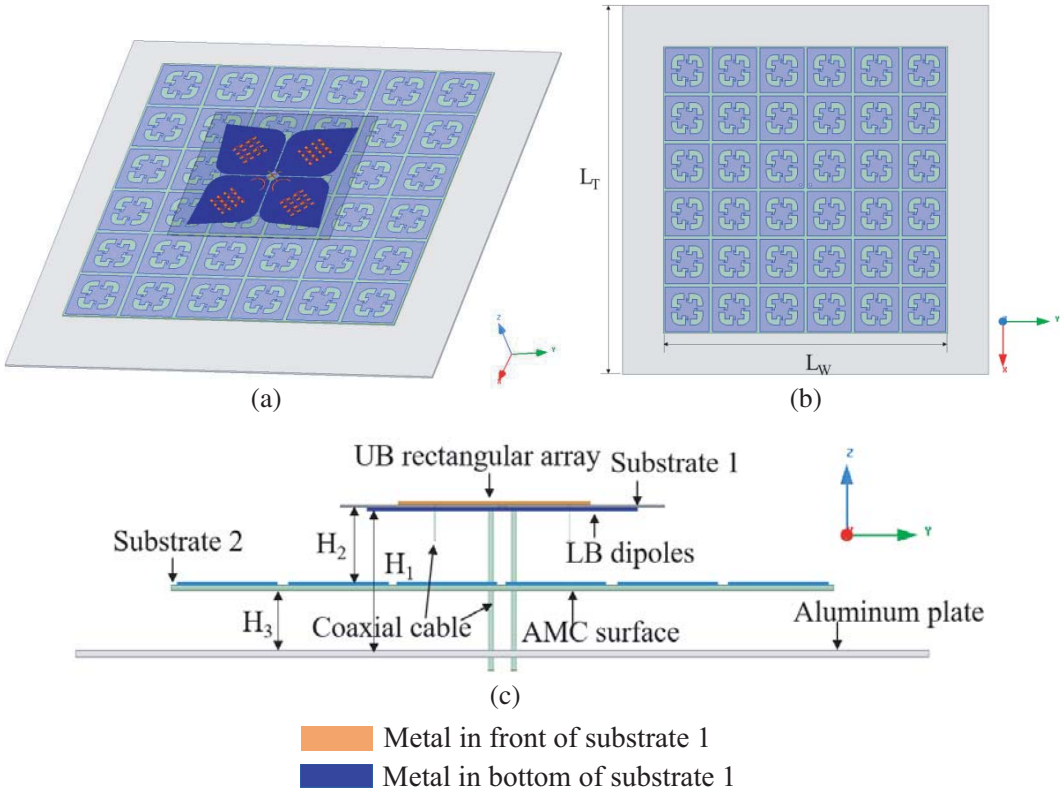

Figure 11. Configuration of low-profile AOA unit. (a) Perspective view. (b) Top view of AMC reflector. (c) Side view. ($H_1 = 45$ mm, $H_2 = 23.5$ mm, $H_3 = 20$ mm).

The prototype of the proposed AOA backed by AMC reflector was fabricated to verify the proposed design as shown in Figure 12. The network analyzer was used to measure the S parameters of the prototype, and the radiation characteristics were measured in an anechoic chamber. The simulated and measured S-parameters of proposed antenna unit are shown in Figure 13. The impedance bandwidths of AOA element are 38.2% (0.7–1.03 GHz) with $S_{nn} < -14$ dB and 10.7% (24.25–27 GHz) with $S_{nn} < -10$ dB. The isolations given by $|S_{21}|$ and $|S_{34}|$ are more than 25 dB and 40 dB for LB and

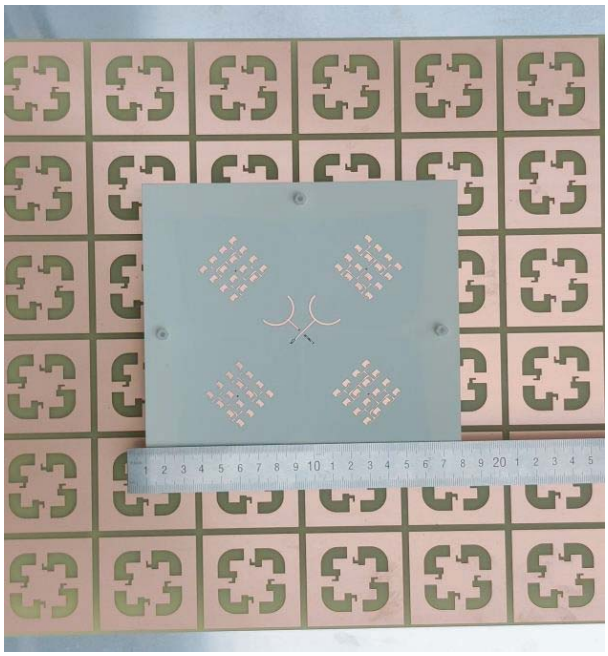

Figure 12. Prototype of the proposed low-profile AOA unit.

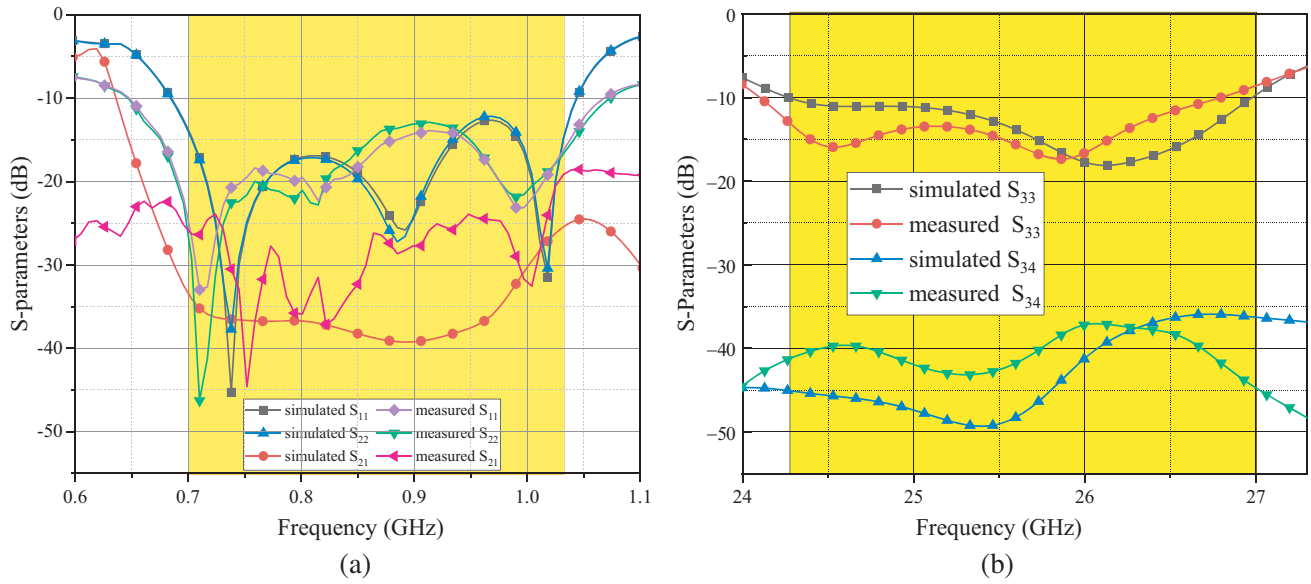

Figure 13. Simulated and measured S-parameters of the AOA unit. (a) Lower-band. (b) Upper-band.

UB, respectively.

Since the radiation pattern of the low-profile AOA is symmetrical on the V-plane (xoz) and H-plane (yoz) in the LB with $\pm 45°$ dual-polarized polarization mode, only the main polarization and cross-polarized radiation directions of the V-plane are given in the LB. Figures 14(a), (c), (e) show the LB radiation patterns of the low-profile AOA antenna unit at 0.7 GHz, 0.8 GHz, and 0.9 GHz, respectively. It can be found that the forward-backward ratio (FBR) is greater than 20 dB in the whole LB. As the frequency increases, the cross-polarization ratio in the maximum radiation direction deteriorates, but it is still greater than 15 dB in the entire lower-frequency operating band. Since the UB antenna arrays of AOA are linearly polarized, the radiation patterns of the V plane and the H

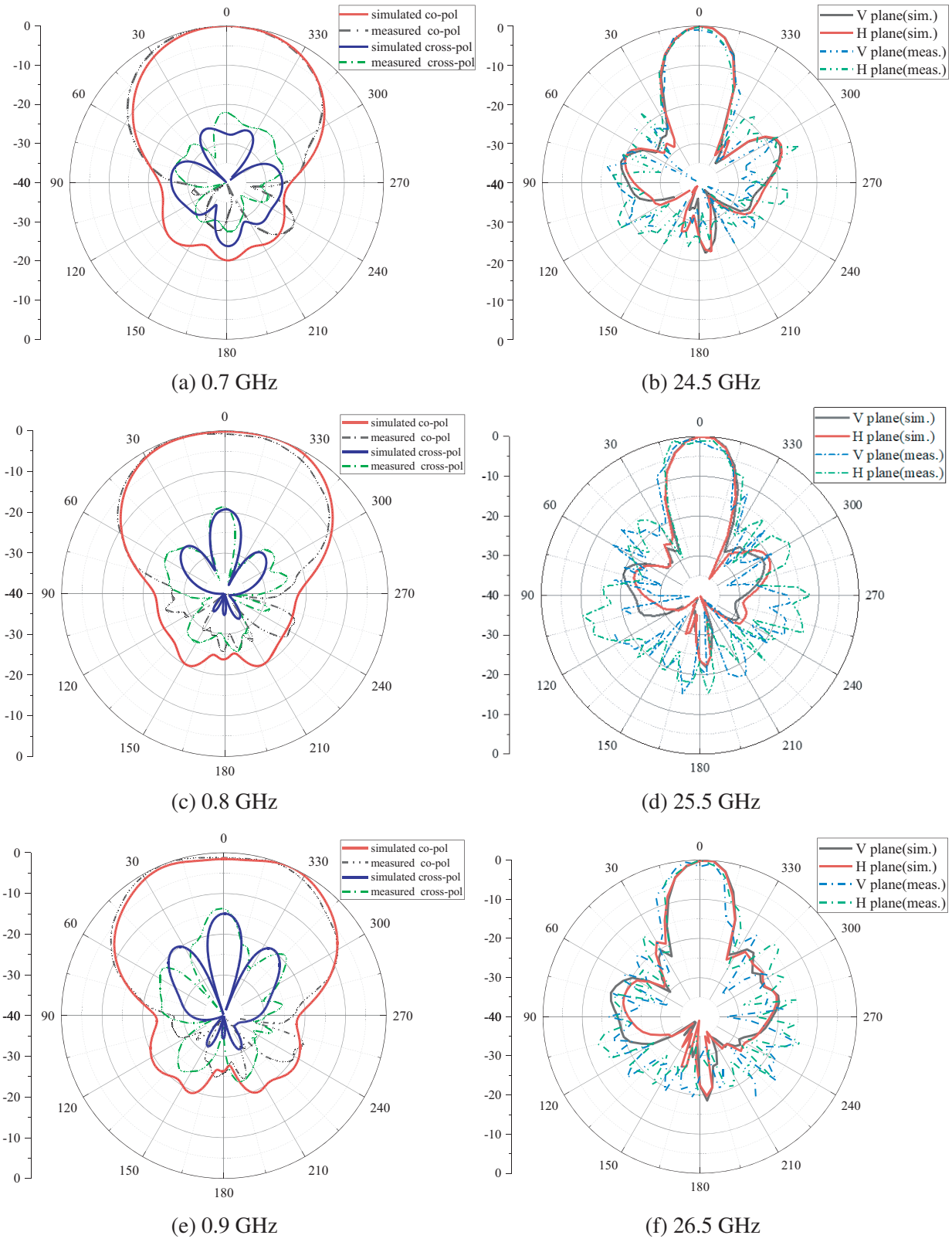

Figure 14. Simulated and measured patterns of the AOA unit. (a), (c), (e) For lower-band. (b), (d), (f) For upper-band.

plane are given in the UB. Figures 14(b), (d), (f) show the V-plane and H-plane radiation patterns of the low-profile AOA antenna unit in the UB of 24.5 GHz, 25.5 GHz, and 26.5 GHz, respectively. The antenna sidelobe level in the UB range is $-20\,\text{dB} \pm 1.5\,\text{dB}$. The beamwidth in UB is $20° \pm 2°$. The FBR in UB is greater than 20 dB. The radiation pattern of the antenna remains basically stable in both upper band and lower one, and the measured results are in good agreement with the simulation ones.

Figure 15 shows the measurement and simulation gains of the low-profile AOA antenna in the maximum radiation direction ($\theta = 0°$) of LB and UB, respectively. The average gain of this antenna at LB is 10.2 dBi, and the average gain at UB is 17.3 dBi. The results show that the measured gain

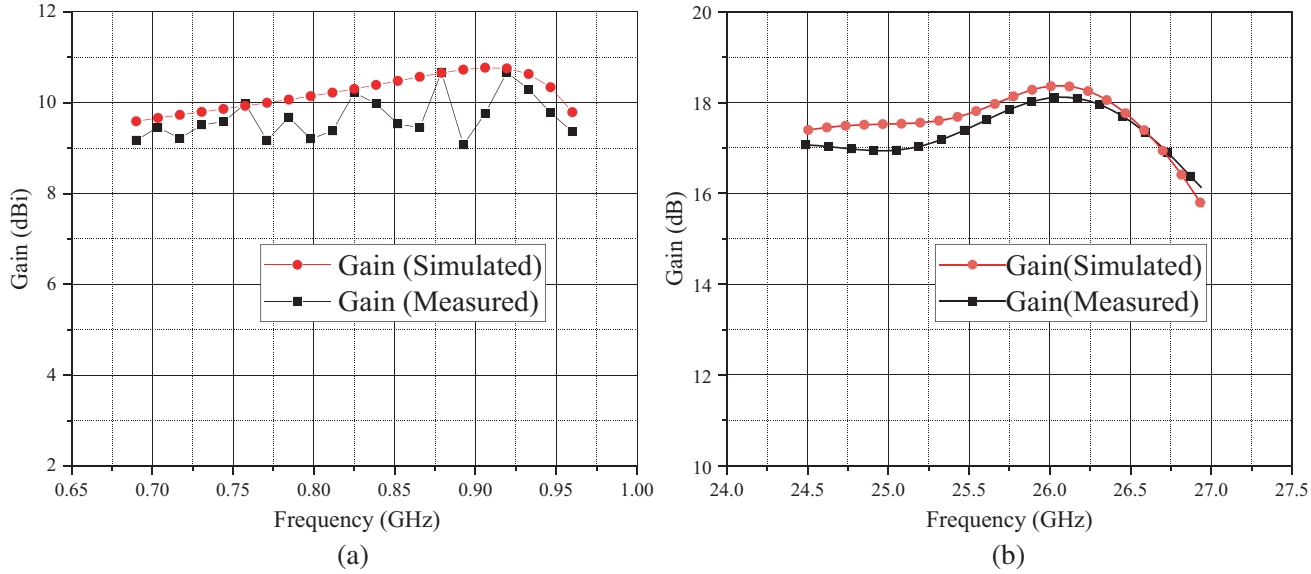

Figure 15. Simulated and measured gains of the AOA unit. (a) Lower-band. (b) Upper-band.

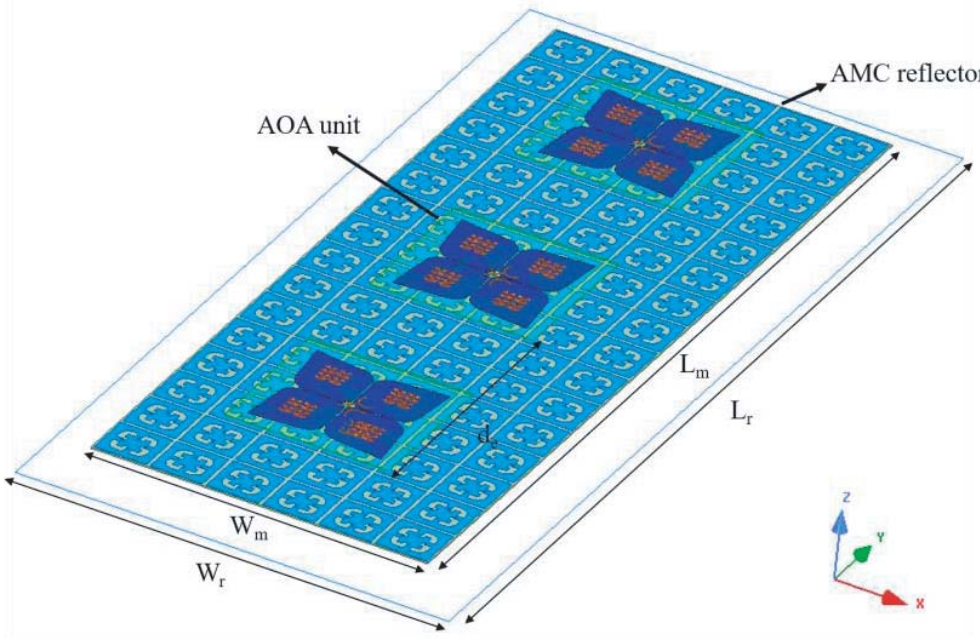

Figure 16. Configuration of AOA antenna array. ($W_r = 448\,\text{mm}$, $W_m = 348\,\text{mm}$, $L_r = 1028\,\text{mm}$, $L_m = 928\,\text{mm}$, $d_e = 290\,\text{mm}$).

is slightly smaller than the simulated gain, which is caused by the insertion loss of the low-frequency power splitter and the high-frequency SMA interface.

4.2. Low-Profile AOA Array

As shown in Figure 16, the proposed low-profile AOA array consists of three AOA elements arranged in a line according to the array element spacing of 290 mm (0.8λ), and an AMC reflector is below the antenna array. The overall size of the array is $1028 \times 448 \times 45\,\text{mm}^3$.

In order to verify the proposed design, a three-element low profile AOA array is fabricated, and the prototype is depicted in Figure 17. The six LB dual-polarized ports of the AOA array are connected by two 1/4 power dividers according to the different polarization directions, and the remaining two ports are connected to the 50 Ω load to achieve matching. The twelve UB single-polarized ports of the AOA array are led out by the SMA interface and connected to the coaxial line.

Figure 18(a) shows the measured and simulated S-parameters of the three-element low-profile AOA antenna array at the two dual-polarized ports of LB. The simulated impedance bandwidth can reach 38.2% in the frequency range of 0.7–1.03 GHz ($S_{nn} < -14$ dB). The isolation of different polarization

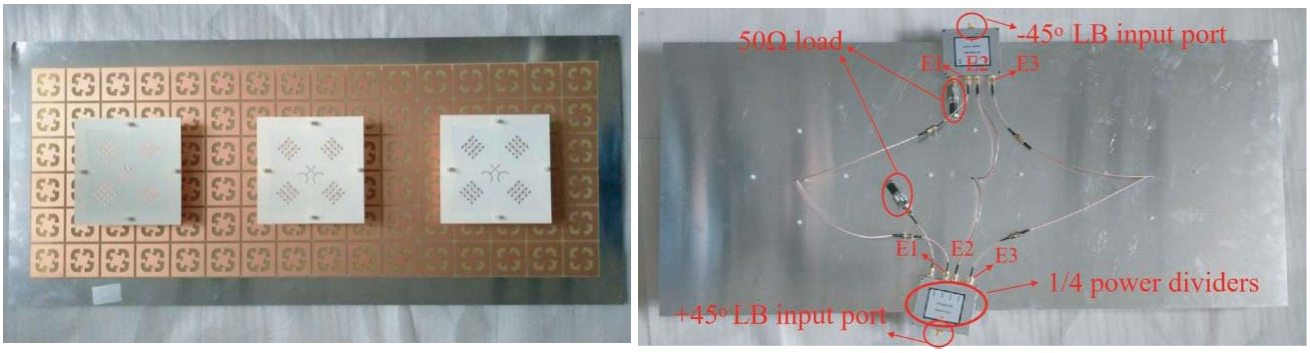

(a) (b)

Figure 17. Prototype of three-element AOA antenna array. (a) Top view. (b) Bottom view.

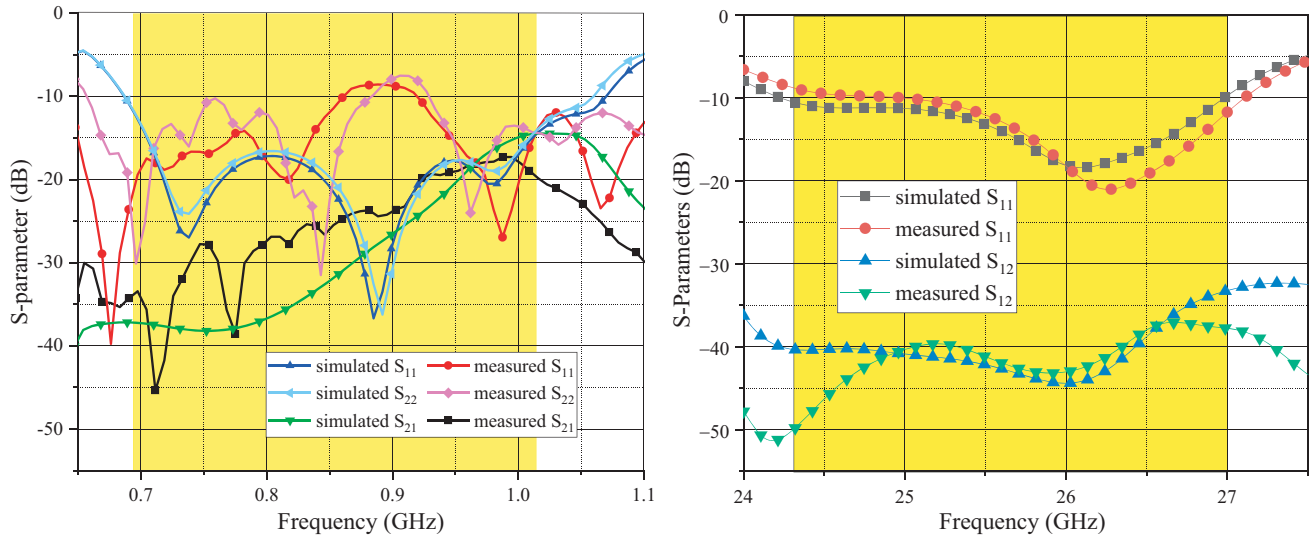

(a) (b)

Figure 18. Simulated and measured S-parameters of three-element AOA antenna array in (a) lower-band; (b) upper-band.

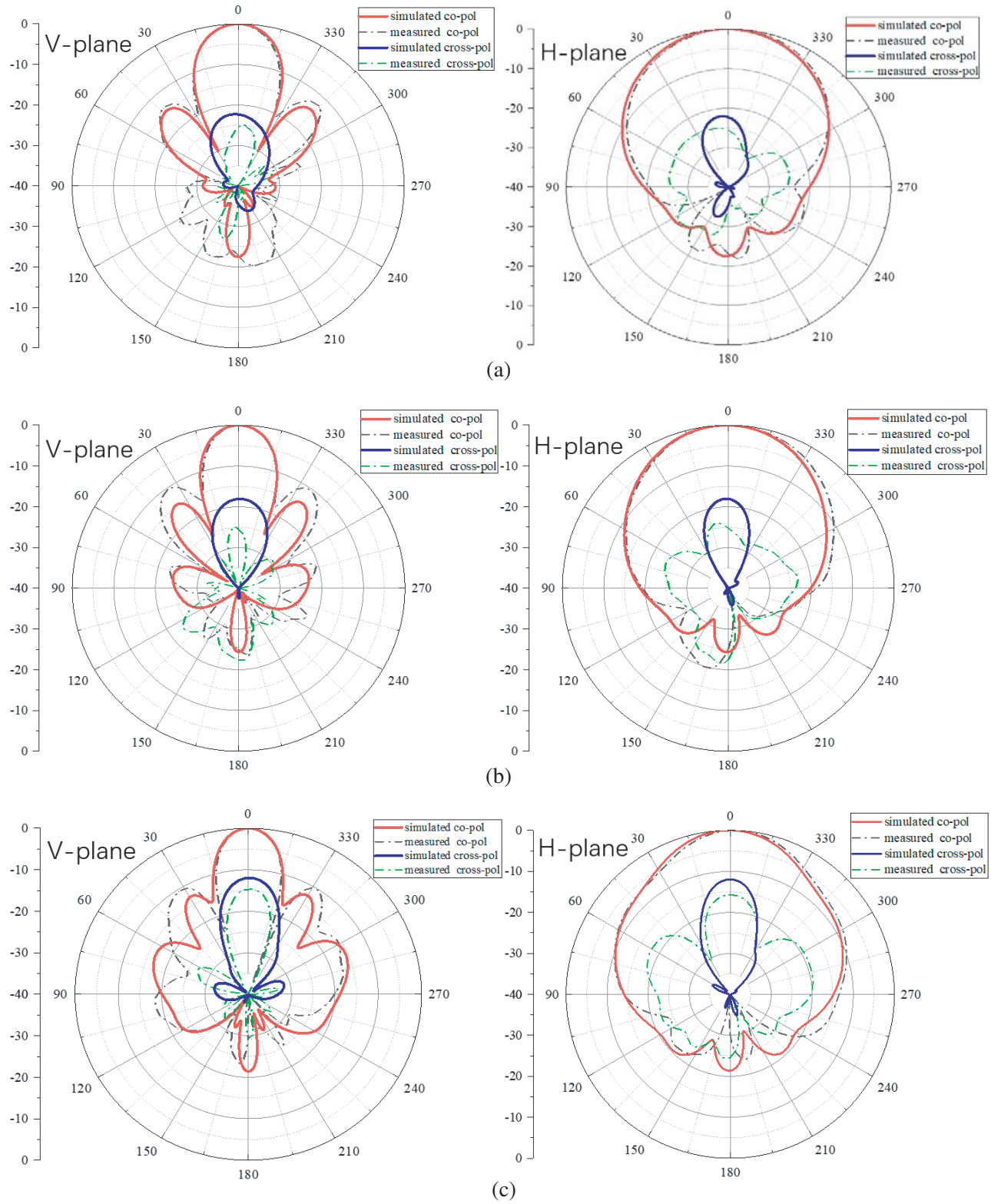

Figure 19. Simulated and measured patterns of three-element AOA antenna array at lower-band. (a) $f = 0.7$ GHz. (b) $f = 0.8$ GHz. (c) $f = 0.9$ GHz.

ports is greater than 15 dB in this frequency band. The 12 UB arrays are symmetrically deployed on the LB dipole antennas, of which performance is mainly related to the local arm of the LB dipoles. The measured and simulated S-parameters of two UB arrays on the middle AOA element are shown in Figure 18(b). The simulated results agree with the measured ones. Since the UB arrays are located on different arms of the LB dipole antenna, the isolation between two adjacent UB ports is more than 30 dB. It is also found that the impedance matching of UB arrays is not influenced by the extension of AMC area.

Measured and simulated V-plane and H-plane radiation patterns of the three-element low-profile AOA array at 0.7, 0.8, and 0.9 GHz are given in Figure 19. The half power beamwidths (HPBWs) in the

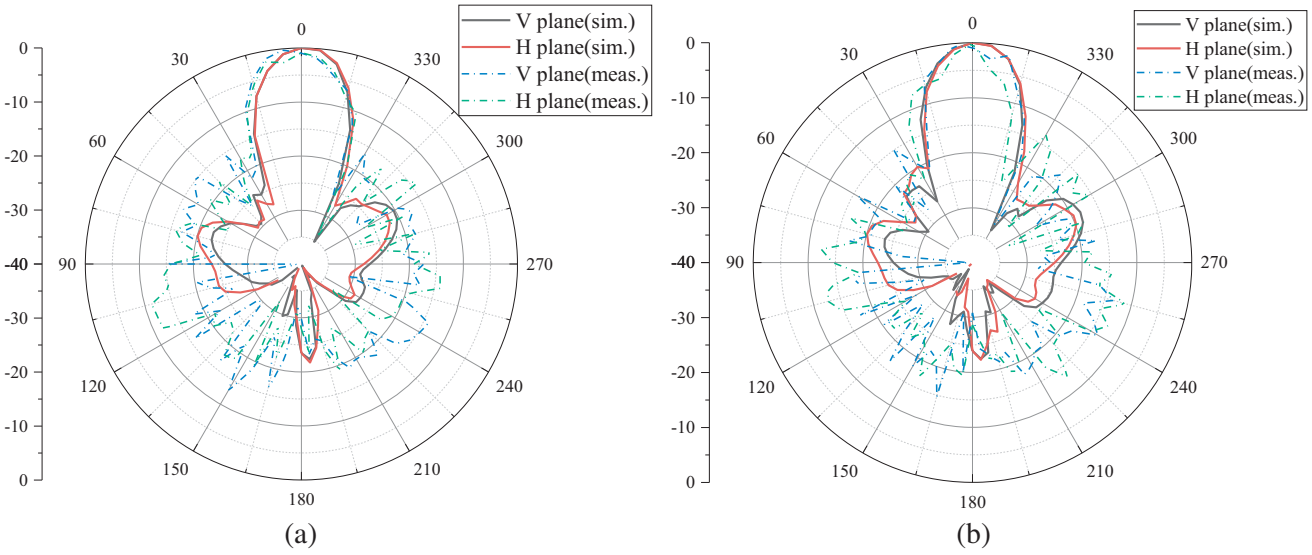

Figure 20. Simulated and measured patterns of AOA antenna array at upper-band. (a) $f = 25.5$ GHz. (b) $f = 26$ GHz.

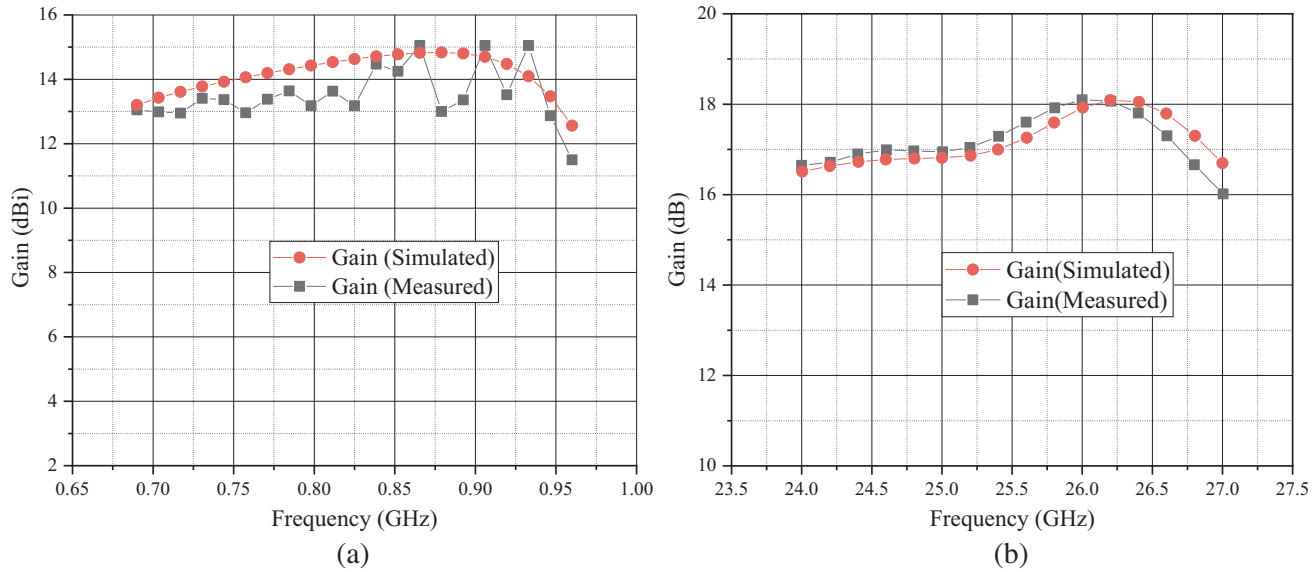

Figure 21. Simulated and measured gains of the proposed three-element AOA antenna array at (a) lower-band; (b) upper-band.

H-plane for these three frequency points are 65°, 54°, and 46°, respectively. The FBR is greater than 20 dB in the whole LB. The cross-polarization ratio deteriorates as the frequency increases and drops to −12 dB at 0.9 GHz. All the UB arrays are fed independently. Figure 20 shows the simulated and measured patterns of AOA array in upper band. The sidelobe level in the UB range is $-20\,\text{dB} \pm 4\,\text{dB}$. The beamwidth is $20° \pm 2°$. The FBR is greater than 20 dB. The average gains of the AOA array in LB and UB are 14.2 dBi and 17.3 dBi, as shown in Figure 21. Table 1 shows the comparison between proposed antenna and other multi-frequency antennas. It can be found that the proposed AOA takes the advantage of larger frequency ratio, higher gain, and lower profile height.

Table 1. Comparison of different multi-band antenna.

Ref.	Frequency (GHz)	Ratio	Impedance BW (%)	Peak Gain (dBi)	Process	Electrical Dimension	Profile Height
[9]	0.83/2.2	2.7	31.6/45.5	9.5/8.9	Embedded	$0.44\lambda_a \times 0.44\lambda_a$	$0.25\lambda_a$
[10]	0.89/1.94	2.18	17.8/23.7	9.138/12.4	Embedded	$0.5\lambda_a \times 0.5\lambda_a$	$0.22\lambda_a$
[21]	2.4/24	1	30.8/4.67	6.8/18.2	DRA integration	$0.192\lambda_a \times 0.192\lambda_a$	$0.187\lambda_a$
[22]	5.2/24	4.6	1.93/2.03	3.93/6.2	Double-layer PCB	$0.363\lambda_a \times 0.363\lambda_a$	Without reflector
[23]	4/60	15	85/13.3	4/7	Single-layer PCB	$0.39\lambda_a \times 0.39\lambda_a$	Without reflector
This Work	0.85/25.5	3	38.2/10.7	1.75/18.25	Single-layer PCB	$0.383\lambda_a \times 0.383\lambda_a$	$0.125\lambda_a$

(Notes: λ_a is the wavelength of the lower operation band).

5. CONCLUSION

In order to meet the application requirements of the coexistence of multi-standard communication systems, a low-profile dual-band composite structure AOA base station antenna unit is designed. The LB dipole antenna radiator serves as the ground of the UB array. The LB and UB radiators share a same dielectric substrate and coexist parasitically. The AMC reflector is loaded on the back of the overall antenna to reduce the profile height of the antenna from the original 90 mm to 45 mm. The simulated and measured results show that the bandwidths of the proposed dual band AOA are 38.2% and 10.7%, respectively. Good impedance matching and stable radiation characteristics are achieved in both operated frequency bands. Based on the above design, a three-element low-profile AOA antenna array was fabricated and measured. Due to the stable radiation performance in multiple bands and low profile, the proposed low-profile AOA base station antenna can be applied to 4G/5G communication systems.

ACKNOWLEDGMENT

This work is supported by the Science and Technology Research Program of Chongqing Municipal Education Commission [grant No. KJQN202000623], National Natural Science Foundation of China [grant No. 61871063, 41606203], and the Chongqing Basic Science and Frontier Technology Research Project (cstc2017jcyjAX0193).

REFERENCES

1. Rappaport, T. S., et al., "Millimeter wave mobile communications for 5G cellular: It will work!," *IEEE Access*, Vol. 1, 335–349, 2013.
2. Gulur Sadananda, K., M. P. Abegaonkar, and S. K. Koul, "Gain equalized shared-aperture antenna using dual-polarized ZIM for mmWave 5G base stations," *IEEE Antennas and Wireless Propagation Letters*, Vol. 18, No. 6, 1100–1104, Jun. 2019.
3. Hong, W., K. Baek, Y. Lee, Y. Kim, and S. Ko, "Study and prototyping of practically large-scale mmWave antenna systems for 5G cellular devices," *IEEE Communications Magazine*, Vol. 52, No. 9, 63–69, Sep. 2014.
4. Zhang, Y. M., H. Liu, et al., "A novel millimeter-wave backward to forward scanning periodic leaky-wave antenna based on two different radiator types," *Progress In Electromagnetics Research*, Vol. 168, 3138, 2020.
5. Hong, W., "Solving the 5G mobile antenna puzzle: Assessing future directions for the 5G mobile antenna paradigm shift," *IEEE Microwave Magazine*, Vol. 18, No. 7, 86–102, Dec. 2017.
6. Arya, A. K., et al., "Shark-fin antenna for railway communications in LTE-R, LTE, and lower 5G frequency bands," *Progress In Electromagnetics Research*, Vol. 167, 83–94, 2020.
7. Feng, B. T., et al., "A dual-wideband double-layer magnetoelectric dipole antenna with a modified horned reflector for 2G/3G/LTE applications," *International Journal of Antennas and Propagation*, Vol. 2013, 1–9, 2013.
8. Yang, L., et al., "A dual-wideband dual-polarized directional magneto-electric dipole antenna," *Microwave and Optical Technology Letters*, Vol. 59, No. 5, 1128–1133, May 2017.
9. Zhang, H., Y. Jiao, and Z. Weng, "A novel dual-wideband directional dipole antenna with double reflecting floors," *IEEE Antennas and Wireless Propagation Letters*, Vol. 16, 1941–1944, 2017.
10. Lu, W., G. Liu, K. F. Tong, and H. Zhu, "Dual-band loop-dipole composite unidirectional antenna for broadband wireless communications," *IEEE Transactions on Antennas and Propagation*, Vol. 62, No. 5, 2860–2866, May 2014.
11. Wu, R. and Q. Chu, "A compact, dual-polarized multiband array for 2G/3G/4G base stations," *IEEE Transactions on Antennas and Propagation*, Vol. 67, No. 4, 2298–2304, Apr. 2019.
12. He, Y., Z. Pan, X. Cheng, Y. He, J. Qiao, and M. M. Tentzeris, "A novel dual-band, dual-polarized, miniaturized and low-profile base station antenna," *IEEE Transactions on Antennas and Propagation*, Vol. 63, No. 12, 5399–5408, Dec. 2015.
13. Lan, J., Z. Yu, J. Zhou, and W. Hong, "An aperture-sharing array for (3.5, 28) GHz terminals with steerable beam in millimeter-wave band," *IEEE Transactions on Antennas and Propagation*, Vol. 68, No. 5, 4114–4119, May 2020.
14. Feng, L. Y. and K. W. Leung, "Dual-frequency folded-parallel-plate antenna with large frequency ratio," *IEEE Transactions on Antennas and Propagation*, Vol. 64, No. 1, 340–345, Jan. 2016.
15. Lian, R., Z. Wang, Y. Yin, J. Wu, and X. Song, "Design of a low-profile dual-polarized stepped slot antenna array for base station," *IEEE Antennas and Wireless Propagation Letters*, Vol. 15, 362–365, 2016.
16. Ge, L. and K. M. Luk, "A magneto-electric dipole antenna with low-profile and simple structure," *IEEE Antennas and Wireless Propagation Letters*, Vol. 12, 140–142, 2013.
17. Tang, H., C. Tong, and J. Chen, "Differential dual-polarized filtering dielectric resonator antenna," *IEEE Transactions on Antennas and Propagation*, Vol. 66, No. 8, 4298–4302, Aug. 2018.
18. Liu, Y., S. Wang, X. Wang, and Y. Jia, "A differentially fed dual-polarized slot antenna with high isolation and low profile for base station application," *IEEE Antennas and Wireless Propagation Letters*, Vol. 18, No. 2, 303–307, Feb. 2019.
19. Alhalabi, R. A. and G. M. Rebeiz, "High-efficiency angled-dipole antennas for millimeter-wave phased array applications," *IEEE Transactions on Antennas and Propagation*, Vol. 56, No. 10, 3136–3142, Oct. 2008.

20. Raad, H. R., A. I. Abbosh, H. M. Al-Rizzo, and D. G. Rucker, "Flexible and compact AMC based antenna for telemedicine applications," *IEEE Transactions on Antennas and Propagation*, Vol. 61, No. 2, 524–531, Feb. 2013.
21. Feng, L. Y. and K. W. Leung, "Dual-fed hollow dielectric antenna for dual-frequency operation with large frequency ratio," *IEEE Transactions on Antennas and Propagation*, Vol. 65, No. 6, 3308–3313, Jun. 2017.
22. Sun, Y. and K. W. Leung, "Substrate-integrated two-port dual-frequency antenna," *IEEE Transactions on Antennas and Propagation*, Vol. 64, No. 8, 3692–3697, Aug. 2016.
23. Wang, D. and C. H. Chan, "Multiband antenna for WiFi and WiGig communications," *IEEE Antennas and Wireless Propagation Letters*, Vol. 15, 309–312, 2016.